Available online at www.sciencedirect.com

SciVerse ScienceDirect

Ceramics International 39 (2013) 7869–7877

CERAMICS INTERNATIONAL

www.elsevier.com/locate/ceramint

Effect of YF_3 on the phase stability and sinterability of hydroxyapatite—Partially stabilized zirconia composites

Anıl Aykul[a], Isil Kutbay[a], Zafer Evis[b], Metin Usta[a,*]

[a]Department of Materials Science and Engineering, Gebze Institute of Technology, Gebze, Kocaeli 41400, Turkey
[b]Department of Engineering Sciences, Middle East Technical University, Ankara 06800, Turkey

Received 23 January 2013; received in revised form 13 March 2013; accepted 14 March 2013
Available online 26 March 2013

Abstract

Pure hydroxyapatite (HA), HA and partially stabilized zirconia composites (PSZ) with YF_3 and HA–PSZ composite containing 5 wt% PSZ without YF_3 were sintered in air at 900 °C, 1100 °C and 1300 °C for 1 h. The reactions and transformation of the phases in the composites were determined by X-ray diffraction. All the composites with or without YF_3 showed desirable thermal stability below 1300 °C and besides various amounts of $CaZrO_3$, any amount of tri-calcium phosphate (TCP) was not observed. Above 1100 °C, composites with YF_3 showed higher thermal stability than the composites without YF_3. On the other hand, pure HA started to decompose and TCP was observed at 1300 °C. Composites with YF_3 showed improved thermal stability than the composite containing 5 wt% PSZ without YF_3 and pure HA at lower sintering temperatures such as 900 °C and 1100 °C. However, it was observed that the increasing amount of YF_3 addition caused negative effect on the thermal stability of the composites. 5ZHA composites with YF_3 showed the highest relative density among all of the composites with or without YF_3.

Keywords: A. Sintering; C. Thermal properties; D. Apatite; D. YF_3

1. Introduction

Hydroxyapatite ($Ca_{10}(PO_4)_6(OH)_2$, HA) is a biocompatible and bioactive ceramic [1–4]. HA has an efficient influence on repairing damaged bone because of its similarity to inorganic part of bone [5–7]. However, there are several restrictions for the usage of HA due to its poor mechanical properties [8–13].

Various methods [7,10,12–17] were used to improve the mechanical properties of HA. Among these methods, reinforcing of HA with another ceramic [14–16,18–20] such as zirconia (ZrO_2) which has high strength and fracture toughness, is a promising method [2,3,5,6,8–10,17,21–25]. However, there are some restrictions for reinforcing HA with ZrO_2. One of them could be the polymorphic transformation of ZrO_2 from tetragonal to monoclinic phase during the cooling process of sintered HA–ZrO_2 composites. This phase transformation mechanism introduces large volume change into composite matrix. This change is sufficient to exceed elastic and fracture limits, and consequently to cause cracking of the ceramics [17]. Therefore, additives such as CaO, MgO and Y_2O_3 can be dissolved in ZrO_2 to minimize this phase transformation that can cause large volume change. When 8% Y_2O_3 was added to ZrO_2, fully stabilized zirconia was obtained instead of monoclinic phase at room temperature (RT). However, when the lower amount of Y_2O_3 exists in ZrO_2, partially stabilized zirconia (PSZ) occurs at RT. In contrast, small degree of this volume expansion provides higher fracture toughness, which is called transformation toughening mechanism [2]. According to previous works, it was found that the excellent mechanical properties were obtained for approximately 3% addition of Y_2O_3 into ZrO_2 [26].

HA decomposes to β-TCP approximately at 1200 °C and α-TCP at ~1300 °C as seen in Reaction 1 [27–30]:

$$Ca_{10}(PO_4)_6(OH)_{2(1-x)} \rightarrow 3Ca_3(PO_4)_2 + CaO + (1-x)H_2O \quad (1)$$

Decomposition of HA seen in Reaction 1 takes place well below 1300 °C and HA starts to decompose to β-TCP in the range of 1100–1150 °C and α-TCP in the range of 1150–1250 °C in the presence of ZrO_2 [12,31,32]. When bioinert ZrO_2 is added to HA as a reinforcing compound, it can

*Corresponding author. Tel.: +90 262 605 2655.
E-mail address: ustam@gyte.edu.tr (M. Usta).

0272-8842/$ - see front matter © 2013 Elsevier Ltd and Techna Group S.r.l. All rights reserved.
http://dx.doi.org/10.1016/j.ceramint.2013.03.048

diminish the biocompatibility and bioactivity of HA [27–30]. Moreover, HA reacts with ZrO_2 as seen in Reaction 2 [2]:

$$Ca_{10}(PO_4)_6(OH)_2+ZrO_2 \rightarrow 3Ca_3(PO_4)_2+CaZrO_3+H_2O \quad (2)$$

During this reaction, HA decomposes into β/α-TCP and a second phase of $CaZrO_3$ in the HA–ZrO_2 composites. Hence, decomposition rate of HA to β/α-TCP increases as the amount of ZrO_2 increases in the composites. HA–ZrO_2 composite decomposition reaction is at ~1300 °C.

Although several studies have characterized the HA–PSZ composites and the effect of YF_3 on hot-pressed HA and monoclinic zirconia composites [21], effect of YF_3 on the phase stability and sinterability of HA–PSZ composites were investigated in this study for the first time. In the present work, pure HA, HA–PSZ composites with or without YF_3 were prepared and sintered at 900 °C, 1100 °C, and 1300 °C for 1 h. Composites were characterized by density, X-ray diffraction (XRD) and scanning electron microscopy (SEM) in order to determine the effect of YF_3 as a sintering agent on the phase formation and sinterability of HA–PSZ composites.

2. Materials and methods

The materials used in this research were composites of HA–PSZ with the addition of YF_3. The abbreviations, description and the composition of the samples of interest to the present study are shown in Table 1.

HA was synthesized by mixing reagent grades of calcium nitrate ($Ca(NO_3)_2 \cdot 4H_2O$) and di-ammonium hydrogen phosphate ($(NH_4)_2HPO_4$) solutions in the alkaline pH region [27,32]. 0.6 M $Ca(NO_3)_2 \cdot 4H_2O$ and 0.3 M $(NH_4)_2HPO_4$ were separately dissolved in distilled water to obtain a Ca/P ratio of 1.67. Then, ammonia was added into the solutions to bring their pH level to a level of 11–12. Then, $Ca(NO_3)_2 \cdot 4H_2O$ solution was added into the $(NH_4)_2HPO_4$ solution in a drop wise manner and pH of the final mixture was kept at 11–12. Following the stirring of the mixture for 24 h, the mixture was left to aging for 2-days. Then, it was filtered with a fine filter paper and a wet cake was obtained. The wet cake was dried in the furnace at 200 °C overnight to remove the excess water. The powders of the PSZ (3% Y_2O_3–97% ZrO_2) (Zirconia Sales Inc.) were then mixed with HA and reagent grade of YF_3 powders. To accomplish this, the dried HA particles were ground to 75 μm size (−200 mesh) powders using an agate mortar and pestle. They were then calcined at 900 °C for 1 h and mixed with PSZ and YF_3 powders by ball milling. Mixed powders were sintered in air at 900 °C, 1100 °C, and 1300 °C for 1 h in a high temperature box furnace. They were heated at rate of 20 °C/min and hold for 1 h at the sintering temperatures and then cooled to RT at rate of 3 °C/min in the furnace.

Table 1
Abbreviation and composition of the samples.

Name	Abbreviation	Composition
Hydroxyapatite and partially stabilized zirconia composites	HA	%100HA
	5ZHA	%5PSZ+%95HA
	5ZHA0.5F	%5PSZ+%94.5HA+%0.5YF_3
	5ZHA1F	%5PSZ+%94HA+%1 YF_3
	5ZHA2.5F	%5PSZ+%92.5HA+%2.5 YF_3
	10ZHA0.5F	%10PSZ+%89.5HA+%0.5 YF_3
	10ZHA1.F	%10PSZ+%89HA+%1 YF_3
	10ZHA2.5F	%10PSZ+%87.5HA+%2.5 YF_3
	20ZHA0.5F	%20PSZ+%79.5HA+%0.5 YF_3
	20ZHA1F	%20PSZ+%79HA+%1 YF_3
	20ZHA2.5F	%20PSZ+%77.5HA+%2.5 YF_3

The bulk density of the sintered samples was determined by measuring the weight and volume of the sintered composites. The theoretical density (ρ_t) of the composites (components a, b, and c) was calculated from the known weights, W and densities, ρ by the following formula [33]:

$$\rho_t(g/cm^3) = \frac{W_a + W_b + W_c}{\left(\frac{W_a}{\rho_a}\right) + \left(\frac{W_b}{\rho_b}\right) + \left(\frac{W_c}{\rho_c}\right)} \quad (3)$$

where component "a" is PSZ, component "b" is HA and/or TCP and component "c" is YF_3. Density of HA and TCP were assumed to be the same for the simplicity of composite density calculation. Theoretical densities of the PSZ, HA, and YF_3 were used as 6.04, 3.156, and 4.01 g/cm^3, respectively.

All the samples were pulverized using an agate mortar and pestle before the XRD characterization. After the pulverizing, they were pressed onto a dimpled quartz glass. Then, they were characterized by a BRUKER-ADVANCE D8 XRD diffractometer with a Cu-Kα radiation at 40 kV/40 mA at 1.54178 Å. Each sample was scanned from 20 to 70° in 2θ with a step size of 0.02° and scanning rate of 3° min^{-1}. The hexagonal lattice parameters of HA were calculated by successive approximations according to standard procedures [34]. The volume of the each unit cell was calculated by the following formula $V=2.589a^2c$ [35]. To determine the phases present in the samples, XRD peak positions were compared with the Joint Committee on Powder Diffraction Standards (JCPDS) PDF files [36].

To determine the decomposition of HA into TCP, the relative amounts of phases (wt%) were determined from the most intense XRD peaks of the HA and α-/β-TCP [34,37]. It is assumed that the concentrations (wt%) of HA and TCP phases are proportional to their peak heights in the mixtures. First the ratio R_O of the peak heights of HA to that of α- or β-TCP was determined for mixtures of known concentrations of HA and α- or β-TCP. Lower limit of detection was about 1 wt% of the known mixture of HA and TCP. It was found that the ratio R_O did not depend on the relative amounts of HA and TCP; the values of R_O found were 1.755 for $R_O=I_H/I_\beta$ and $R_O=I_H/I_\alpha=2.217$, where I_H, I_β and I_α are the XRD peak heights for HA, β- and α-TCP, respectively in mixtures of known concentrations. Then, according to sintering temperatures (900 °C, 1100 °C, and 1300 °C), %HA decomposed to α and β-TCP in the

composites was calculated by the following formula:

$$W_H/W_\beta = R/R_O \quad (4)$$

where W_H and W_β are the weight fractions of HA and β-TCP, respectively. A similar formula for mixtures of HA and α-TCP, with W_α substituted for W_β, was used. Moreover, hexagonal lattice parameters and unit cell volume change of HA in the HA–PSZ composites were calculated by successive approximations according to standard procedures [34].

Sample surfaces were examined by a JEOL JSM-840A SEM at 7–15 kV to determine the grain size of the composites. Samples were coated with gold by a POLARON-SC7610 Sputtering vacuum before the examination in the SEM. Grain size was determined by the intercept method. A 20 cm circumference circle was used to determine grain sizes of the samples. The following formula was used to determine the grain sizes from the SEM micrographs [38].

$$G_{ave} = L/NM \quad (5)$$

where G_{ave} is the average grain size, L the circumference of the circle (20 cm), N the number of intersections along 20 cm circumference line and M is the magnification.

3. Results

The relative densities of HA and all of the composites sintered at 900 °C, 1100 °C and 1300 °C for 1 h are shown in Fig. 1(a,b,c,d). In Fig. 1a, pure HA samples showed the intense increase of relative density value with increasing the sintering temperature up to 1100 °C and then slowly increasing the temperature up to 1300 °C.

The relative densities of the 5ZHA composite samples with or without YF_3 are shown in Fig. 1b. According to Fig. 1b, 5ZHA0.5F, 5ZHA1F, 5ZHA2.5F showed similar relative densities at 1100 °C and their relative densities increased with increasing the temperature up to 1100 °C. 5ZHA composite without YF_3 did not have the density as high as the other three composites had at 1100 °C. This relative density difference between 5ZHA composites with and without YF_3 can be denoted as thermal stability effect of YF_3 on the thermal sinterability of 5ZHA composites. Even though, significant differences were not observed for 5ZHA composites with YF_3 as a sintering agent, 5ZHA2.5F composite showed the highest relative densities at higher sintering temperatures such as 1300 °C among the 5ZHA composites with YF_3 addition.

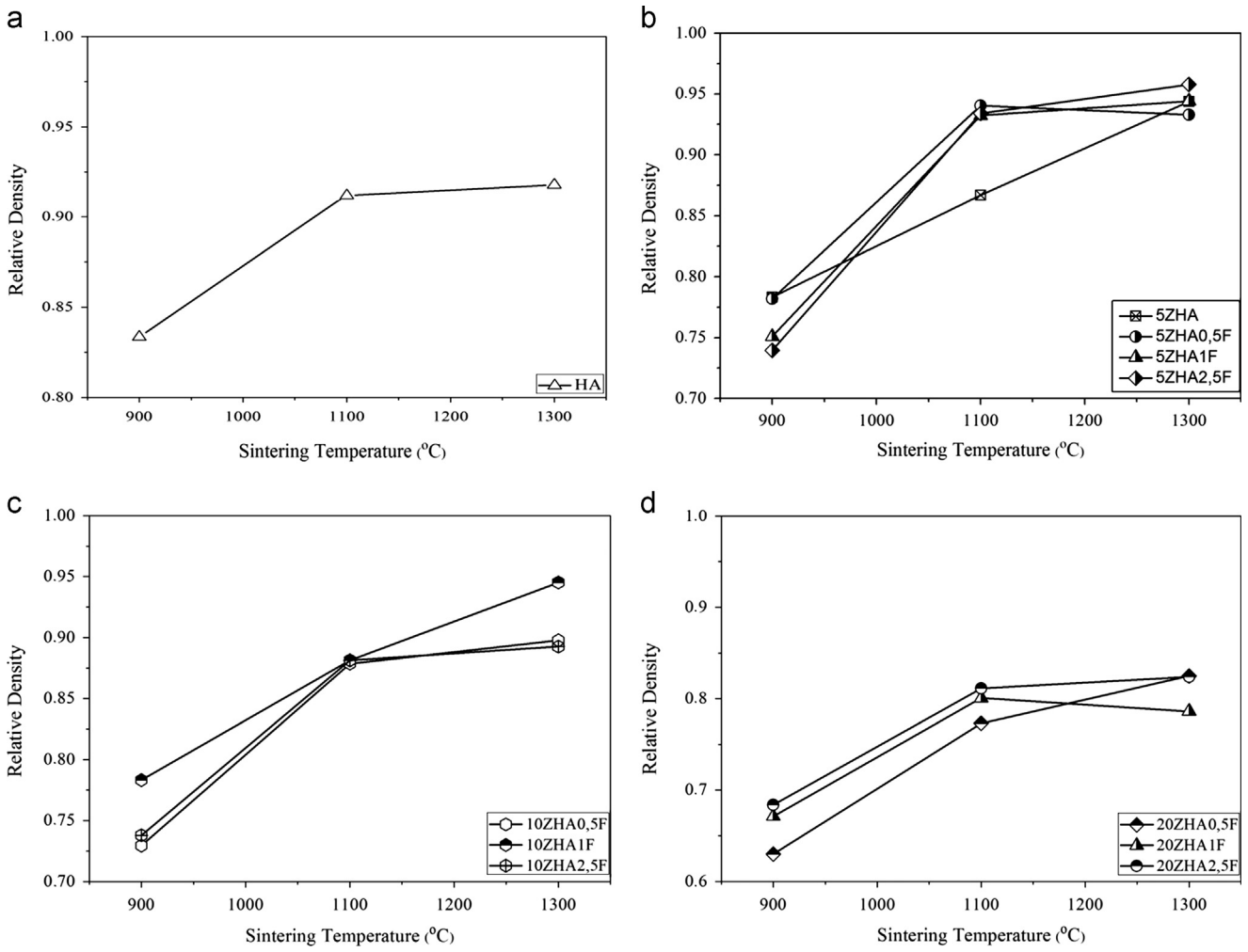

Fig. 1. Effect of various sintering temperatures on relative densities of the samples: (a) HA; (b) 5ZHA composites; (c) 10ZHA composites; (d) 20ZHA composites.

10ZHA composites with YF_3 showed similar sinterability as 5ZHA composites with YF_3 addition according to Fig. 1c. The most prominent difference between Fig. 1b and c is that the reduction for relative density value of 10ZHA2.5F composite is lower than the reduction for relative density value 5ZHA2.5F at sintering temperature of 1300 °C.

According to comparison between Fig. 1c and d, similar densification behavior for 20ZHA0.5F and 10ZHA0.5F was observed. Between 10ZHA and 20ZHA composites, highest relative density values for 20ZHA composites were obtained by increasing the sintering temperatures which showed significant reduction compared to 10ZHA composites. Therefore, increasing amount of PSZ content in the composites could be the reason for this significant reduction of the highest density value.

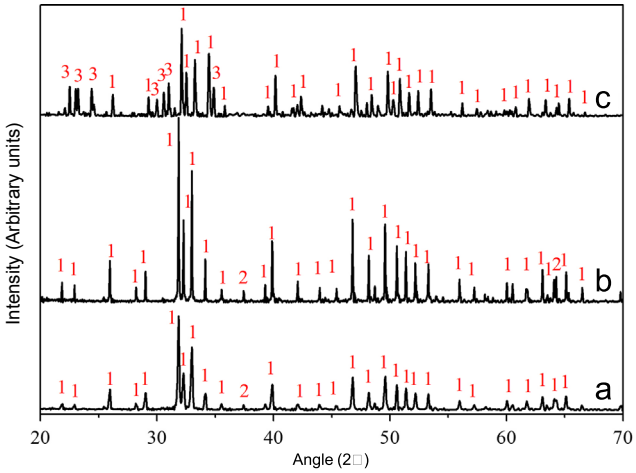

Fig. 2. XRD patterns of (a) pure HA sintered at 900 °C for 1 h; (b) pure HA sintered at 1100 °C for 1 h; (c) pure HA sintered at 1300 °C for 1 h. (Phases: 1: HA; 2: CaO; 3: α-TCP).

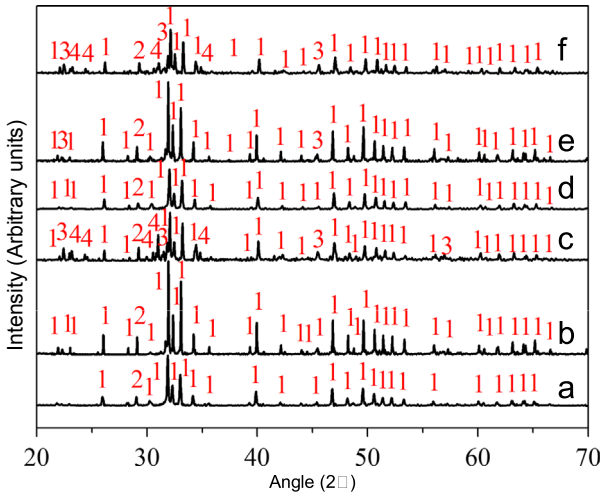

Fig. 3. XRD patterns of (a) 5ZHA sintered at 900 °C for 1 h; (b) 5ZHA sintered at 1100 °C for 1 h; (c) 5ZHA sintered at 1300 °C for 1 h; (d) 5ZHA0.5F sintered at 900 °C for 1 h; (e) 5ZHA0.5F sintered at 1100 °C for 1 h; (f) 5ZHA0.5F sintered at 1300 °C for 1 h. (Phases: 1: HA; 2: t-ZrO_2; 3: $CaZrO_3$; 4: α-TCP).

XRD patterns of all the samples sintered at 900 °C, 1100 °C and 1300 °C for 1 h are presented in Figs. 2–6. XRD patterns of the samples were compared with JCPDS files for HA (JCPDS #9-432), β-TCP (JCPDS #9-169); α-TCP (JCPDS #9-348), CaO (JCPDS #48-1467), $CaZrO_3$ (JCPDS #35-0790), and t-ZrO_2 (JCPDS #50-1089).

In general, it was observed that the decomposition of HA to α-TCP and β-TCP was accelerated by increasing the sintering temperature (especially at 1300 °C). Furthermore, increasing percentage of PSZ in all the composites degraded thermal stability of pure HA and HA–PSZ composites and the composites containing 20 wt% PSZ showed the thermal

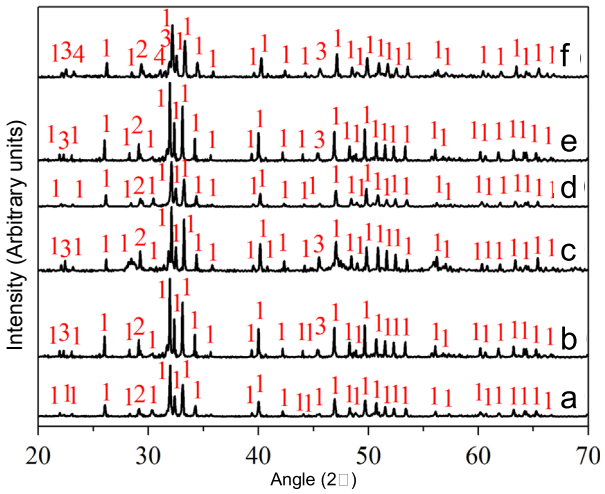

Fig. 4. XRD patterns of (a) 5ZHA1F sintered at 900 °C for 1 h; (b) 5ZHA1F sintered at 1100 °C for 1 h; (c) 5ZHA1F sintered at 1300 °C for 1 h; (d) 5ZHA2.5F sintered at 900 °C for 1 h; (e) 5ZHA2.5F sintered at 1100 °C for 1 h; (f) 5ZHA2.5F sintered at 1300 °C for 1 h. (Phases: 1: HA; 2: t-ZrO_2; 3: $CaZrO_3$; 4: α-TCP).

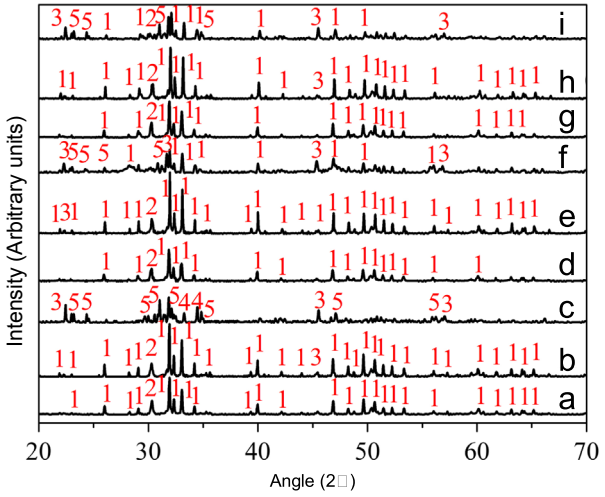

Fig. 5. XRD patterns of (a) 10ZHA0.5F sintered at 900 °C for 1 h; (b) 10ZHA0.5F sintered at 1100 °C for 1 h; (c) 10ZHA0.5F sintered at 1300 °C for 1 h; (d) 10ZHA1F sintered at 900 °C for 1 h; (e) 10ZHA1F sintered at 1100 °C for 1 h; (f) 10ZHA1F sintered at 1300 °C for 1 h; (g) 10ZHA2.5F sintered at 900 °C for 1 h; (h) 10ZHA2.5F sintered at 1100 °C for 1 h; (i) 10ZHA2.5F sintered at 1300 °C for 1 h. (Phases: 1: HA; 2: t-ZrO_2; 3: $CaZrO_3$; 4: β-TCP; 5: α-TCP).

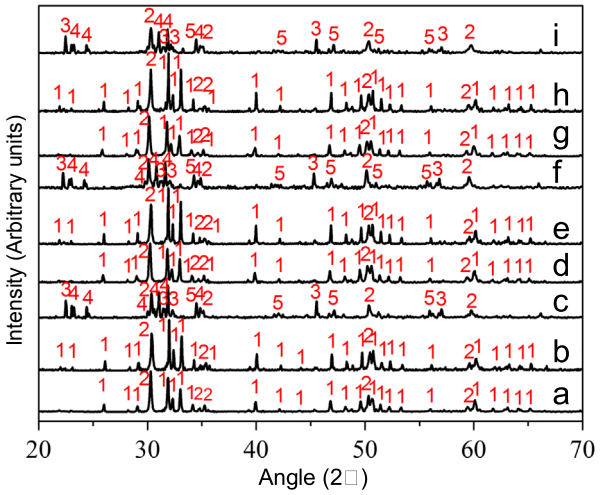

Fig. 6. XRD patterns of (a) 20ZHA0.5F sintered at 900 °C for 1 h; (b) 20ZHA0.5F sintered at 1100 °C for 1 h; (c) 20ZHA0.5F sintered at 1300 °C for 1 h; (d) 20ZHA1F sintered at 900 °C for 1 h; (e) 20ZHA1F sintered at 1100 °C for 1 h; (f) 20ZHA1F sintered at 1300 °C for 1 h; (g) 20ZHA2.5F sintered at 900 °C for 1 h; (h) 20ZHA2.5F sintered at 1100 °C for 1 h; (i) 20ZHA2.5F sintered at 1300 °C for 1 h. (Phases: 1: HA; 2: t-ZrO_2; 3: $CaZrO_3$; 4: β-TCP; 5: α-TCP).

instability even if the amount of YF_3 content was increased from 0.5 to 2.5 wt%, respectively. When the sintering of pure HA, HA–PSZ composites with YF_3 and 5ZHA was carried out below 1300 °C, small amount of CaO was observed in pure HA and small amount of $CaZrO_3$ was observed in HA–PSZ composites. As the sintering temperature was increased to 1300 °C, HA started to decompose to second phases (e.g. α-TCP). Hence, α-TCP was observed in almost all composites with the smallest value for 5ZHA1F sintered at 1300 °C and β-TCP was observed in 20ZHA0.5F, 20ZHA1F and 20ZHA2.5F sintered at 1300 °C. Moreover, highest thermal stability for 5ZHA1F among others at higher sintering temperature of 1300 °C was verified with decomposition percentage of HA to TCP (Table 2). Percentage of HA decomposed to α and β-TCP of the samples is shown in Table 2. In addition, HA decomposed at high values to both β- and α-TCP in 20ZHA composites at 1300 °C (Table 2). It was observed that increasing the YF_3 amount in 20ZHA composites increased the decomposition rate of HA to second phases such as α and β-TCP at 1300 °C.

When sintering temperature was increased from 1100 to 1300 °C, composites with 2.5 wt.% YF_3 showed higher tendency to decompose than the composites containing less amount of YF_3 as well as accelerated F–OH ion substitution between HA and YF_3. 20ZHA composites containing 0.5 wt% YF_3 showed better thermal stability than the composites containing 1 and 2.5 wt% YF_3 at 1300 °C. Addition of YF_3 improved the thermal stability of the HA–PSZ composites at low sintering temperatures such as 900°C and 1100 °C. However, when the excess amount of YF_3 content exists in HA–PSZ composites, thermal stability of HA–PSZ composites were negatively affected at higher sintering temperatures. Consequently, it can be easily inferred from XRD results that YF_3 content has two specific effect on HA–PSZ

Table 2
%HA decomposed to TCP in pure HA and HA–ZrO_2 composites with or without YF_3.

Sample ID	Sintering temperature (°C)		
	900 °C	1100 °C	1300 °C
HA	0	6.3	45.6
5ZHA	0	21.5	54.1
5ZHA0.5F	0	10.9	35.7
5ZHA1F	0	8.9	19.01
5ZHA2.5F	0	12.5	23.9
10ZHA0.5F	0	8.8	66.4
10ZHA1F	0	5.5	48.6
10ZHA2.5F	0	9.6	55.8
20ZHA0.5F	0	0	63.1
20ZHA1F	0	0	65.4
20ZHA2.5F	0	13.7	69.6

Table 3
Hexagonal lattice parameters and unit cell volume change of pure HA and HA–ZrO_2 composites.

Sample ID	Sintering temperatures (°C)	Lattice parameters (Å)		Unit cell volume (Å^3)
		a	c	
HA	900	9.4054	6.8708	1573.6
	1100	9.408	6.8691	1574.1
	1300	9.3463	6.8265	1543.9
5ZHA	900	9.4074	6.8726	1574.7
	1100	9.3934	6.8611	1567.4
	1300	9.3598	6.8462	1552.8
5ZHA0.5F	900	9.3695	6.841	1554.8
	1100	9.3966	6.8629	1568.8
	1300	9.3441	6.8346	1544.9
5ZHA1F	900	9.3774	6.854	1560.4
	1100	9.3815	6.8625	1563.7
	1300	9.3528	6.8344	1547.8
5ZHA2.5F	900	9.3506	6.8382	1547.9
	1100	9.3809	6.8648	1564.03
	1300	9.3286	6.825	1537.7
10ZHA0.5F	900	9.3917	6.8603	1566.6
	1100	9.3947	6.8635	1568.4
	1300	9.3553	6.8504	1552.3
10ZHA1F	900	9.3988	6.8695	1571.1
	1100	9.3818	6.8567	1562.5
	1300	9.3826	6.8653	1564.7
10ZHA2.5F	900	9.3938	6.869	1569.3
	1100	9.3647	6.85	1555.3
	1300	9.3461	6.8368	1546.1
20ZHA0.5F	900	9.3966	6.8654	1569.4
	1100	9.3697	6.8463	1556.1
	1300	–	–	–
20ZHA1F	900	9.4086	6.8811	1577.03
	1100	9.3881	6.8644	1566.4
	1300	–	–	–
20ZHA2.5F	900	9.4124	6.8966	1581.9
	1100	9.3855	6.8638	1565.3
	1300	–	–	–

composites. The first effect of YF_3 on HA–PSZ composites is YF_3 deficiency. When YF_3 deficiency occurs, the optimal F–OH ion substitution between HA and YF_3 cannot occur. Second effect is the addition of excess YF_3 to HA–PSZ composites. In this case, decomposition of HA is accelerated and the amount of water, which is given away by the chemical reaction (2) between HA and YF_3, increases. According to XRD results of HA–ZrO_2 composites, it was found out that the optimum amount percentage of YF_3 was 1 wt%.

Hexagonal lattice parameters and unit cell volume change of HA in HA–PSZ composites are shown Table 3. Lattice parameter (a and c) changes of pure HA, 5ZHA, and 5ZHA, 10ZHA, 20ZHA with different amount percentage of YF_3 composites that occur during the pressureless air sintering at different temperatures are presented, and also unit cell volume changes of pure HA and HA–PSZ composites are presented in Table 3. According to Table 3, when the unit cell volume changes between HA and HA–PSZ composites is compared, it is observed that the ion substitution of F- for OH^- between HA and YF_3 during the sintering of HA–PSZ composites causes lower unit cell volume. In addition, the ion substitution of ZrO^{2+} for Ca^{2+} between HA and PSZ during the sintering of the composites causes higher unit cell volume. In general, it could be easily inferred from both lattice parameter and unit cell volume results that both of lattice parameter and unit cell volume values decrease with increasing amount of YF_3. However, 20ZHA2.5F composite has higher lattice parameter and higher unit cell volume among 20ZHA composites.

SEM micrographs of pure HA, 5ZHA, 5ZHA0.5F, 5ZHA1F and 5ZHA2.5F samples, sintered at 900 °C, 1100 °C and 1300 °C, respectively, are presented in Fig. 7. Average grain sizes determined from the SEM micrographs showed changes in grain size of the composites (Table 4). Especially, for 5ZHA2.5F, the grain size was increased from 135 to 1041 nm

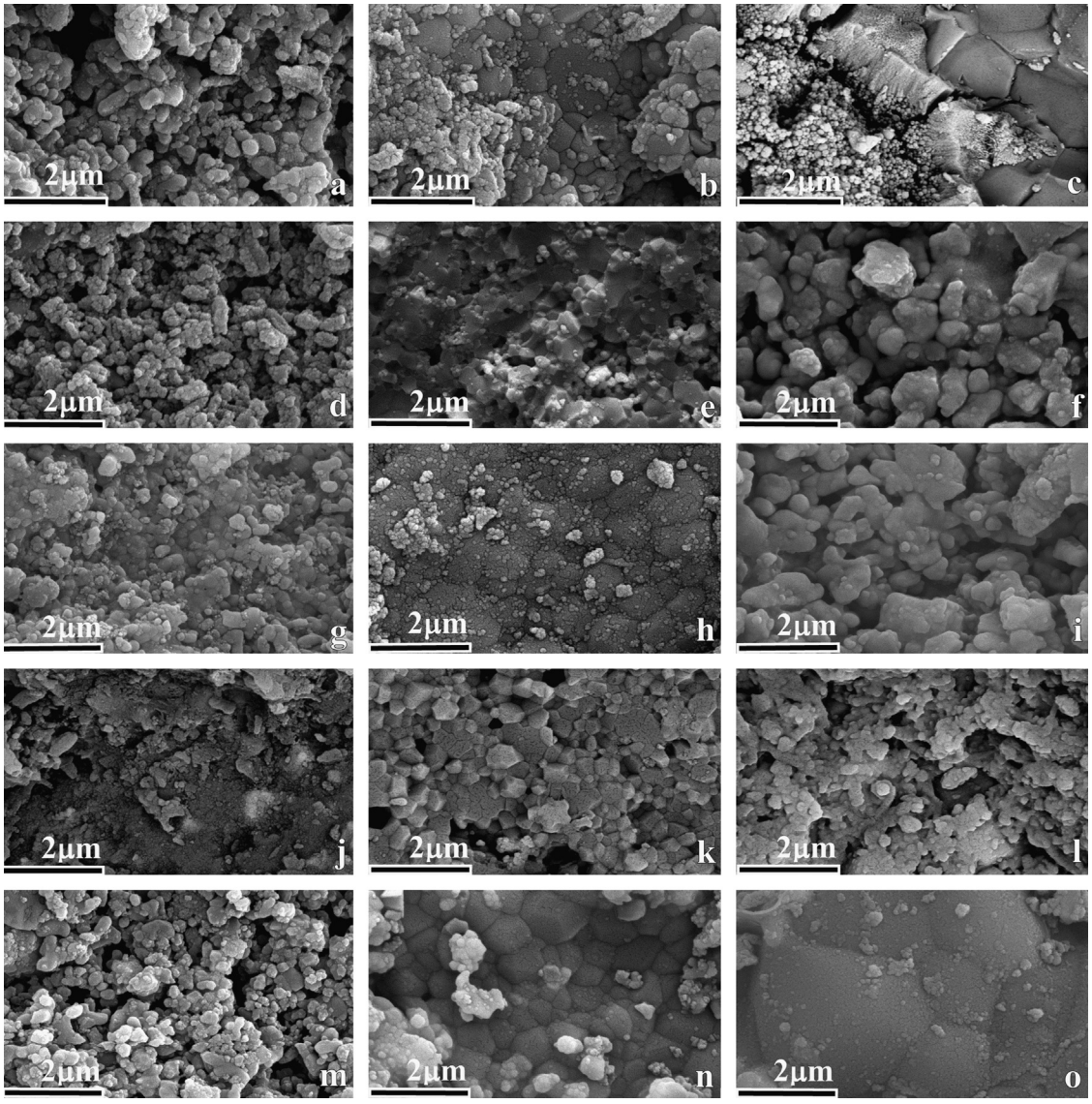

Fig. 7. SEM micrographs of pure HA sintered for 1 h at (a) 900°C, (b) 1100 °C, (c) 1300 °C; 5ZHA sintered for 1 h at (d) 900 °C, (e) 1100 °C, (f) 1300 °C; 5ZHA0.5F sintered for 1 h at (g) 900 °C, (h) 1100 °C, (i) 1300 °C; 5ZHA1F sintered for 1 h at (j) 900 °C, (k) 1100 °C, (l) 1300 °C; 5ZHA2.5F sintered for 1 h at (m) 900 °C, (n) 1100 °C, and (o) 1300 °C.

Table 4
Average grain sizes of the pure HA, 5ZHA, 5ZHA0.5F, 5ZHA1F, 5ZHA2.5F sintered at 900 °C, 1100 °C, 1300 °C for 1 h.

Sintering temperature (°C)	Average grain size (nm)				
	HA	5ZHA	5ZHA0.5F	5ZHA1F	5ZHA2.5F
900	148	130	132	122	135
1100	195	178	271	142	189
1300	328	260	328	183	1041

when sintering temperature was increased from 900°C to 1300 °C. In particular, there was more grain growth in the composites after sintering between 1100 °C and 1300 °C. Similar results were seen for the other HA and HA–PSZ composites (data not shown). 5ZHA1F samples had smaller grain sizes than the other 5ZHA samples (Fig. 7, Table 4) for all of sintering temperatures (900 °C, 1100 °C, and 1300 °C).

Consequently; among 5ZHA and 5ZHA0.5F, 5ZHA1F, 5ZHA2.5F composites, it was observed that HA–PSZ composites with YF_3 showed higher densification than the HA–PSZ composite without YF_3 at 900 °C, 1100 °C and 1300 °C. This situation is determined as the basic influence of YF_3 on the densification of HA–PSZ composites. Moreover, 5ZHA showed lower densification than pure HA at 900 °C and 1300 °C. Therefore, increased proportion of porosity was observed in 5ZHA microstructure at both 900 °C and 1300 °C, because ZrO_2 has a negative influence on densification of HA. However, 5ZHA sintered at 1100 °C had higher crystallinity than pure HA. On the other hand, according to SEM micrograph of HA and 5ZHA, it can be inferred that the growth of HA grains shows little reduction with the increasing sintering temperatures.

All of the HA–PSZ composites with YF_3 showed similar densification characteristics at 900 °C, 1100 °C and 1300°C, respectively. Although 5ZHA0.5F, 5ZHA1F and 5ZHA2.5F did not show enough densification, these composites still had higher densification than that of pure HA at 900 °C. Otherwise, 5ZHA0.5F, 5ZHA1F and 5ZHA2.5F composites did not have enough sinterability at low sintering temperatures such as 900 °C. It seems that the sintering temperature (900 °C) is not sufficient to provide an adequate driving force for a higher densification. Among these composites sintered at 900 °C, 5ZHA1F had the highest densification at this sintering temperature. Grain growth was encountered in both 5ZHA0.5F and 5ZHA2.5F as the sintering temperature was increased from 900 °C to 1300 °C. In contrast, the grain growth was minimized significantly in 5ZHA1F with increasing sintering temperatures. On the other hand, 5ZHA2.5F composite had the best densification among the three composites at 1300°C.

4. Discussion

As seen in Fig. 1b, c, and d, highest densification behavior was observed for 5ZHA with YF_3 among the composite groups. Although % YF_3 addition has a great influence on densification of HA–PSZ, it seems that also % ZrO_2 addition takes an important role in densification of HA–PSZ by accelerating the decomposition of HA as seen in reaction (1). In addition, the increasing ZrO_2 addition reduced relative density value for both 10ZHA and 20ZHA with YF_3 composites. Consequently, lowest relative density values were obtained from 20ZHA with YF_3 composites. This situation could be one of the possible reason why the 5ZHA with YF_3 composite group, which includes the lowest % ZrO_2 content, shows the highest densification. Chemical reaction (2) presents interaction between HA and ZrO_2 [7,23,28]. $CaZrO_3$ is formed when ZrO_2 is added to the HA structure, as seen in reaction (2). This reaction could be the possible reason for reduction of relative density of HA–ZrO_2 composite because of removing of CaO from HA structure and giving away of H_2O. Thus, higher porosity is obtained in the presence of higher amount of ZrO_2 and it leads to the lower relative density [6,29]. When adequate amount of YF_3 was added to HA–PSZ composites, more relative density values were achieved than that of 5ZHA composite without YF_3. Unlike 10ZHA and 20ZHA composites with YF_3, 5ZHA composites with YF_3 showed slight reduction of relative density values above 1100 °C. Moreover, higher relative density value is acquired for 5ZHA1F composite among 5ZHA composites with YF_3. One of the possible reason for this situation could be the influence of adequate amount of YF_3 for elimination of decomposition of HA. The same densification behavior is also observed for 10ZHA composites and the highest relative density is obtained for 10ZHA1F composite. However, the amount of YF_3 required for the highest relative density increased from 1 wt% to 2.5 wt %. It seems that the adequate amount of YF_3 is 2.5 wt% in order to eliminate decomposition of HA with 20 wt% ZrO_2 addition.

The optimum level effect of YF_3 entirely depends on relative amount of YF_3 and t-ZrO_2. The optimum level effect of YF_3 can be well observed for 10ZHA composites. Because both of YF_3 and t-ZrO_2 amounts are sufficient to neutralize their decomposition effects by interacting themselves chemically more than HA. According to XRD patterns; the least decomposition of HA was observed for 5ZHA composites which had YF_3 addition at all the sintering temperatures. Even if 2.5 wt% YF_3 was added to HA–PSZ composite, the destructive effect of YF_3 did not take place because the amount of HA was relatively greater than the YF_3 and as a consequence in contrast to other composites (10ZHA2.5F, 20ZHA2.5F) only small amount of α-TCP was observed for 5ZHA2.5F composite at 1300 °C. However, when the relative amount of both YF_3 and t-ZrO_2 is increased, YF_3 plays more effective role in HA–ZrO_2 composite.

For 10ZHA composites; it was observed that 0.5 wt% addition of YF_3 was insufficient to improve thermal stability of HA–ZrO_2, however, 2.5 wt% addition of YF_3 was far too much than the needed amount. Hence, 10ZHA1F composite showed the highest relative density (Fig. 1.c) value and decomposition rate (Table 2) at 1300 °C among other 10ZHA composites. This situation can be associated with literature [39] that excess amount of Y^{3+} degrades the sinterability and thermal stability of HA–ZrO_2 composites.

The ion substitution of F^- for OH^- between HA and YF_3 consists during the sintering of HA–ZrO_2 composites which include YF_3 as a sintering agent. Moreover, this ion substitution provides higher thermal stability to HA–ZrO_2 composites because F^- ions have smaller atomic radii than that of OH^- ions have. As a result, replacing OH^- ions with smaller one enables to relieve unit cell's stress and makes HA more stable at higher temperatures [7,11,31]. On the other hand, there are some different ion substitutions that take place during the sintering of HA–ZrO_2 composites. The ion substitution of ZrO^{2+} for Ca^{2+} could occur during the sintering process of HA–ZrO_2 composites and unlike the ion substitution of F^- for OH^-, this ion substitution leads to higher lattice parameter and higher unit cell volume, which causes to increase the unit cell's stress [27]. However, the lattice parameter (a) and unit cell volume results for 10ZHA1F composite had greater value than both 10ZHA0.5F and 10ZHA2.5F composites at 1300 °C. The amount of Ca^{2+} for 10ZHA0.5F composite resulted from HA decomposition at 1300 °C led to expansion in unit cell. That is why higher both lattice parameter (a) and unit cell volume value were resulted. 10ZHA2.5F composite had lower both lattice parameter (a) and unit cell volume value than the 10ZHA1F as well. The possible reason for this is that YF_3 mostly interacted with HA and resulted with increased decomposition rate of 10ZHA2.5F composite as well as ion substitution Y^{3+} for Ca^{2+}, as seen supported in Fig. 5.

5. Conclusion

XRD patterns showed the decomposition mechanism of HA to second phases affected by both t-ZrO_2 and YF_3 content ratio in two different ways. t-ZrO_2 has a great impact on decomposition rate of HA. Therefore, higher amount of t-ZrO_2 addition increases the decomposition tendency of HA. In contrast to t-ZrO_2, YF_3 could be either beneficial or destructive. These characteristics mostly depend on its addition amount to composites. In order to benefit from YF_3 content, experimental works should be carried out either under the optimum level of YF_3 or at the optimum level of YF_3. YF_3 interacts with both HA and t-ZrO_2. When this interaction takes place between HA and YF_3, there could be two possible ion substitution process. One of these ion substitution process is F^- for OH^- while the other is Y^{3+} for Ca^{2+}. The second one could be destructive for HA–ZrO_2 composites because of causing Ca^{2+} deficiency, when the excess amount of YF_3 content exists in composite structure. Optimum amount of YF_3 addition helps HA to relieve its stress by replacing OH^- ions with the smaller one (F^-) and makes it more stable at higher sintering temperatures. On the other hand, when the optimum amount of YF_3 is exceeded, the Ca^{2+} deficiency occurs and HA become more prone to decompose at higher sintering temperatures.

Acknowledgments

The authors would like to thank to Mr. A. Sen and Mr. S.L. Aktug for X-ray measurements and Mr. A. Nazim for SEM studies at Gebze Institute of Technology.

References

[1] J. Tian, Preparation of porous hydroxyapatite, Journal of Materials Science 36 (2001) 3061–3066.
[2] A.R. Kmita, A. Slosarczyk, Z. Pazskiewicz, C. Paluszkiewicz, Phase stability of hydroxyapatite–zirconia (HAp–ZrO_2) composites for bone replacement, Journal of Molecular Structure 704 (2004) 333–340.
[3] C.Y. Chiu, H.C. Hsu, W.H. Tuan, Effect of zirconia addition on the microstructural evolution of porous hydroxyapatite, Ceramics International 33 (2007) 715–718.
[4] W. Suchanek, M. Yoshimura, Processing and properties of hydroxyapatite-based biomaterials for use as hard tissue replacement implant, Journal of Materials Research 13 (1998) 94–117.
[5] K. Prabakaran, S. Kannan, S. Rajeswari, Development and characterisation of zirconia and hydroxyapatite composites for orthopaedic applications, Trends in Biomaterials and Artificial Organs 18 (2005) 114–116.
[6] H. Guo, K.A. Khor, Y.C. Boey, X. Miao, Laminated and functionally graded hydroxyapatite/yttria stabilized tetragonal zirconia composites fabricated by spark plasma sintering, Biomaterials 24 (2003) 667–675.
[7] S. Miyatake, Y. Hara, K. Maeda, A. Akamine, M. Eto, K. Yamada, M. Aono, Hydroxyapatite implant for human periodontal osseous defects, Journal of Japanese Society of Periodontology 31 (1989) 318–326.
[8] Z. Evis, M. Usta, I. Kutbay, Improvement in sinterability and phase stability of hydroxyapatite and partially stabilized zirconia composites, Journal of the European Ceramic Society 29 (2009) 621–628.
[9] H.W. Kim, Y.J. Noh, Y.H. Koh, H.E. Kim, H.M. Kim, Effect of CaF_2 on densification and properties of hydroxyapatite–zirconia composites for bio-medical applications, Biomaterials 23 (2002) 4113–4121.
[10] K. Yoshida, K. Hashimoto, Y. Toda, S. Udagawa, T. Kanazawa, Fabrication of structure-controlled hydroxyapatite/zirconia composite, Journal of the European Ceramic Society 26 (2006) 515–518.
[11] L.L. Hench, Bioceramics: from concept to clinic, Journal of the American Ceramic Society 74 (1991) 1487–1510.
[12] K. DeGroot, C. De Putter, P. Smitt, A. Driessen, Mechanical failure of artificial teeth made of dense calcium hydroxyapatite, Science of Ceramics 11 (1981) 433–437.
[13] S. Bose, S. Dasgupta, S. Tarafder, A. Bandyopadhyay, Microwave processed nanocrystalline hydroxyapatite: simultaneous enchancement of mechanical and biological properties, Acta Biomaterialia 6 (2010) 3782–3790.
[14] Y.M. Kong, S. Kim, H.E. Kim, I.S. Lee, Reinforcement of hydroxyapatite bioceramic by addition of ZrO_2 coated with Al_2O_3, Journal of the American Ceramic Society 82 (1999) 2963–2968.
[15] H.W. Kim, Y.M. Kong, Y.H. Koh, H.E. Kim, H.M. Kim, J.S. Ko, Pressureless sintering and mechanical and biological properties of fluor–hydroxyapatite composites with zirconia, Journal of the American Ceramic Society 86 (2003) 2019–2026.
[16] K. Park, T. Vasilosa, Microstructure and mechanical properties of silicon carbide whisker/calcium phosphate composites produced by hot pressing, Materials Letters 32 (1997) 229–233.
[17] V.V. Silva, F.S. Lameiras, R.Z. Domingues, Microstructure and mechanical study of zirconia–hydroxyapatite (ZH) composite ceramics for biomedical applications, Composites Science and Technology 61 (2001) 301–310.
[18] V.V. Silva, R.Z. Domingues, Hydroxyapatite–zirconia composites prepared by precipitation method, Journal of Materials Science: Materials in Medicine 8 (1997) 907–910.
[19] V.V. Silva, F.S. Lameiras, Synthesis and characterization of calcia–partially-stabilized-zirconia–hydroxyapatite composite powders, Materials Characterization 45 (2000) 51–59.
[20] J. Li, B. Fartash, L. Hermansson, Hydroxyapatite–alumina composites and bone-bonding, Biomaterials 16 (1995) 417–422.
[21] Z. Evis, R.H. Doremus, Effect of YF_3 on hot-pressed hydroxyapatite and monoclinic zirconia composites, Materials Chemistry and Physics 105 (2007) 76–79.
[22] Z. Shen, E. Adolfsson, M. Nygren, L. Gao, H. Kawaoka, K. Niihara, Dense hydroxyapatite–zirconia ceramic composites with high strength for biological applications, Advanced Materials 13 (2001) 214–216.

[23] R.R. Rao, T.S. Kannan, Synthesis and sintering of hydroxyapatite–zirconia composites, Materials Science and Engineering 20 (2002) 187–193.
[24] J.M. Wu, T.S. Yen, Sintering of hydroxyapatite–zirconia composite materials, Journal of Materials Science 23 (1988) 3771–3777.
[25] P. Christel, A. Meunier, M. Heller, J.P. Torre, C.N. Peille, Mechanical properties and short-term in vivo evaluation of yttrium-oxide–partially-stabilized-zirconia, Journal of Biomedical Materials Research 23 (1989) 45–61.
[26] Y. Kan, H. Zhang, P. Wang, O.V. Biest, J. Vleugels, Yb_2O_3 and Y_2O_3 co-doped zirconia ceramics, Journal of the European Ceramic Society 26 (2006) 3607–3612.
[27] Z. Evis, Reactions in hydroxyapatite–zirconia composites, Ceramics International 33 (2007) 987–991.
[28] Z. Evis, M. Usta, I. Kutbay, Hydroxyapatite and zirconia composites: effect of MgO and MgF_2 on the stability of phases and sinterability, Materials Chemistry and Physics 110 (2008) 68–75.
[29] K. Morita, S. Ebisu, H. Toda, Y. Shimabukuro, H. Okada, H. Gotou, F. Nishimura, T. Nakamura, S. Takashiba, Y. Nomura, Application of synthetic hydroxyapatite to periodontal therapy, Journal of Japanese Society of Periodontology 31 (1989) 249–255.
[30] A. Finoli, D. McKeel, J. Gerlach, I. Nettleship, Phase transformation behavior of hydroxyapatite foams subject to heat treatment, Biomedical Materials 5 (2010) 1–5.
[31] Z. Evis, R.H. Doremus, Effect of ZrF_4 on hot-pressed hydroxyapatite/monoclinic zirconia composites, Scripta Materialia 56 (2007) 53–56.
[32] Z. Evis, Al^{3+}-doped nano-hydroxyapatites and their sintering characteristics, Journal of the Ceramic Society of Japan 114 (2006) 1001–1004.
[33] Z. Evis, C. Ergun, R.H. Doremus, Hydroxylapatite–zirconia composites: thermal stability of phases and sinterability as related to the $CaO–ZrO_2$ phase diagram, Journal of Materials Science (40-5) (2005) 1127–1134.
[34] B.D. Cullity, Elements of X-ray Diffraction, second ed., Addison-Wesley Publishing Company, Philippines, 411–415.
[35] C. Ergun, T.J. Webster, R. Bizios, R.H. Doremus, Hydroxylapatite with substituted magnesium, zinc, cadmium, and yttrium I. Structure and microstructure, Journal of Biomedical Materials Research 59 (2002) 305–311.
[36] JCPDS, International Centre for Diffraction Data, Newtown Square, Pennsylvania, USA, 2003.
[37] C.R. Hubbard, E.H. Evans, D.K. Smith, The reference intensity ratio, I/I_c, for computer simulated powder patterns, Journal of Applied Crystallography 9 (1976) 169–174.
[38] J.E. Hilliard, Estimating grain size by the intercept method, Metal Progress Data Sheets 84 (1964) 99–102.
[39] B. Basar, A. Tezcaner, D. Keskin, Z. Evis, Improvements in microstructural, mechanical and biocompatibility properties of nano-sized hydroxyapatites doped with yttrium and fluoride, Ceramics International 36 (2010) 1633–1643.